Modelling and Simulation of The BLDC Electric Drive System Using SIMULINK/MATLAB for a Hybrid Vehicle

Technical Report · January 2014

CITATIONS
4

READS
16,549

3 authors:

Mohammad Mahdi Momenzadeh
Universität Paderborn
2 PUBLICATIONS **4** CITATIONS
SEE PROFILE

Abdullah Fathi Ahmed
Universität Paderborn
2 PUBLICATIONS **7** CITATIONS
SEE PROFILE

Amr Tolba
German Aerospace Center (DLR)
2 PUBLICATIONS **4** CITATIONS
SEE PROFILE

UNIVERSITÄT PADERBORN

Die Universität der Informationsgesellschaft

Fachgebiet Leistungselektronik und Elektrische Antriebstechnik
Prof. Dr.-Ing. Joachim Böcker

Modelling and Simulation of

The BLDC Electric Drive System

Using SIMULINK/MATLAB for a Hybrid Vehicle

—Documentation—

Project Seminar

SS 2013

Authors:

Mohammad Mahdi Momenzadeh (mmahdi@mail.uni-paderborn.de)

Abdullah Fathi Ahmed (afaahmed@mail.uni-paderborn.de)

Amr Tolba (amr-90@mail.uni-paderborn.de)

Table of Contents

Table of Figures

1. Introduction

In presence of decaying the resources of fossil fuel and global warming issue, the researchers now investigated for new alternatives. One of these efforts led to the idea of Electric Hybrid Vehicles. The BLDC motors are employed in order to realize the mobility part of the system due to the high efficiency, reliability, low maintenance and easier control implementation.

The prominent feature which makes Brushless DC Motors different from conventional DC motor is the substitution of Electrical commutation system with the mechanical self-commutating analogy. There are two different types of commutations namely Sinusoidal and Trapezoidal commutation which each can be used based on some criteria. The first approach can be used for PMSM since the flux in these kind of motors is distributed in a sinusoidal fashion while one can employ the second method for BLDC motors due to their trapezoidal flux distribution [1] [2]. To implement the electrical commutation for a three phase BLDC motor, a three-phase full-bridge inverter consisting of six electronic switches is required. At this stage, having an electrically commuted BLDC motor, we should come up with an approach to take control of the motor characteristics. Basically, there are two usual applicable methods namely Pulse Width Modulation (PWM) and Space Vector Modulation (SVM). In this project, the PWM method is applied to modulate a control reference signal on a high frequency triangular waveform in order to modify the average voltages given to the motor. The comparison between the two methods is presented in [3].

In the following chapters, the three main blocks of the whole electric drive system of a BLDC motor will be discussed individually. Firstly, the essential principles and mathematical model of the BLDC motor will be presented. In the second part, the electrical commutation of the BLDC motor is developed. Followed by this part, the SIMULINK/MATLAB modeling of the system will be presented. In the last chapter, the computational effort to design the controllers followed by the final results are also discussed.

2. Principle of Brushless Direct Current Motor BLDC

Brushless direct current motors (BLDC) are rapidly gaining popularity due to the absence of brushes in BLDC motor as the name implies and investigating electronic commutation systems rather than mechanical analogy. In addition, they have high efficiency, reliability and require very less maintenance. Furthermore, BLDC motors have several advantages over the conventional brushed DC motors such as higher torque-weight ratio, high dynamic response and better speed vs. torque characteristics [4]. BLDC motors are nowadays used in every sector of market, especially in the areas of appliances production, aeronautics, medicine, consumer and industrial automations. The BLDC motors are kind of permanent magnet synchronous motors (PMSM), which are driven by commutated direct current (DC) voltage [5].

2.1. BLDC Construction

The most common shape of the BLDC motor is the cylindrical shape. This shape and all others include two main parts. The fixed or stationary part which is called stator and the moving part is named rotor. The most popular construction is a rotor, which appears inside the stator. This construction is

popular because placing the nonmoving stator on the outside makes it easy to attach the motor to its surroundings. Moreover, confining the rotor inside the stator provides a natural shield to protect the moving rotor from its surroundings [6].

2.1.1. Stator

The stator of a BLDC motor is made of laminated steel stacked up to hold the windings. Most BLDC motors have three stator windings connected in star manner; however delta connection can also be used in such motors. Each winding is assembled with various coils interrelated to derive a winding. Each of these windings is spread over the stator peripherally to structure a pairs of poles [2].

2.1.2. Rotor

The rotor of BLDC is made of a permanent magnet material mounted on a non-magnetic rotor core or shaft. The number of poles on the rotor varies depending on the application requirements. However, the number of poles is a trade-off between toque and speed. That means the higher number of poles the better torque it produces while it reduces the maximum possible speed [6].

2.2. Working principle

The working principle of BLDC motor is based on the interaction between two magnetic fields which one is on stator, and the other one is on the rotor. To do so, a current is applied in proper direction through the windings of the stator as shown in Figure 2-1. The generated electromagnetic field on the winding is in opposite direction of the magnetic field of the rotor. The created force attraction between these two magnetic fields produces a torque, which is used to move the rotor. In other scenario, if the current is applied in opposite direction the generated force interaction moves the rotor in opposite direction as shown in Figure 2-2.

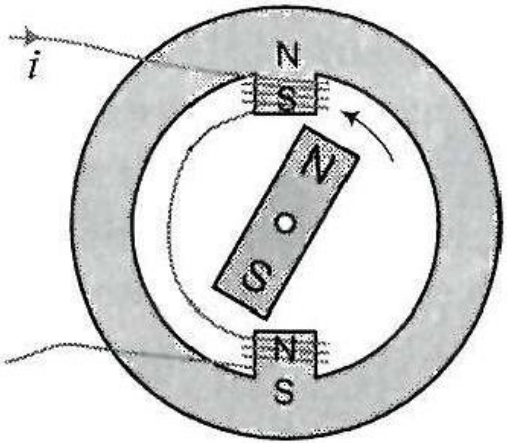

Figure 2-1 Applied current in proper direction [6]

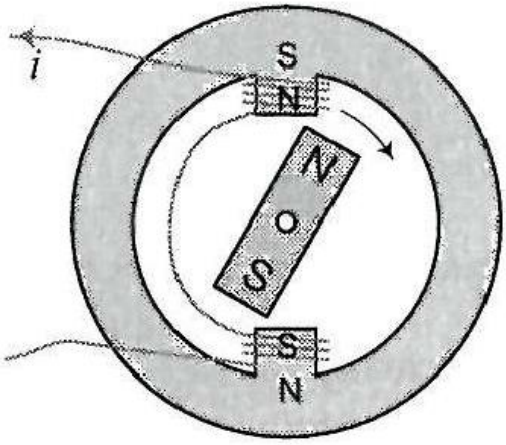

Figure 2-2 Applied current in opposite direction [6]

To keep the rotor moving continuously, it is common to investigate more than one pair of windings as shown in Figure 2-3, which refer to number of phases. For successively rotating, the polarity of poles on stator must be energized and deenergized respectively to attract and repel those of the rotor in commutation process.

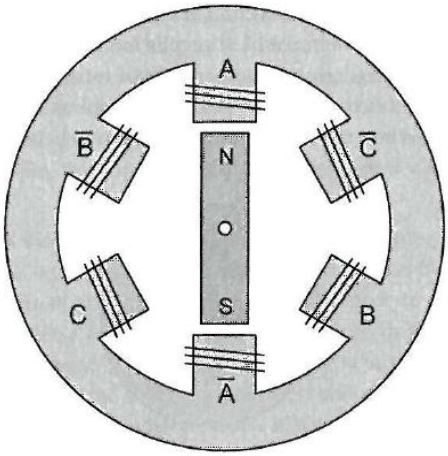

Figure 2-3 Three-phase Motor [6]
The labels A, B and C refer to the phases while the labels with bars refer to the opposite magnet poles, which are faced to the rotor magnet

2.3. Mathematical Model

In this report, three-phase BLDC motor in star connection is proposed. With the assumption that R_a=R_b=R_c=R due to symmetry of three-phase BLDC motor and L_a=L_b=L_c=L=$L_s - M$, the equivalent circuit is arranged as shown in Figure 2-4. Here, the small letters a, b and c denote the phases of the BLDC motor.

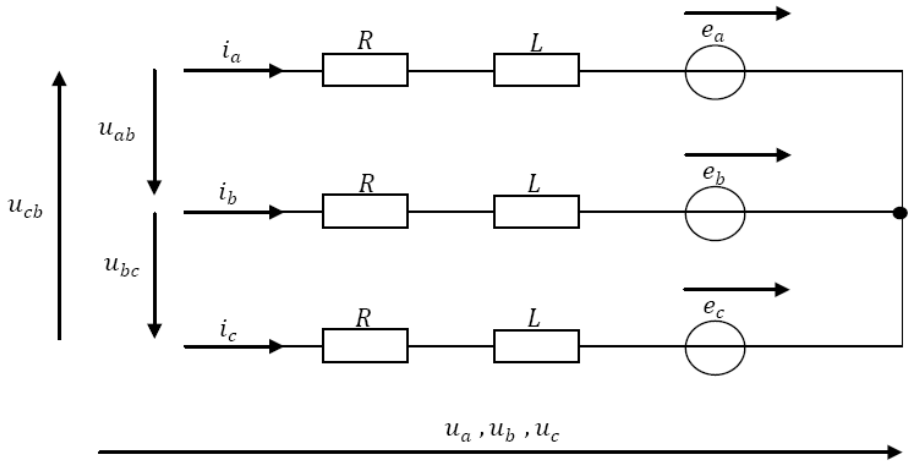

Figure 2-4 The equivalent circuit of three- phase motor star-connection

The following equations describe the equivalent circuit:

$$u_a = Ri_a + L\frac{di_a}{dt} + e_a \qquad \textbf{Equation 2-1}$$

$$u_b = Ri_b + L\frac{di_b}{dt} + e_b \qquad \textbf{Equation 2-2}$$

$$u_c = Ri_c + L\frac{di_c}{dt} + e_c \qquad \textbf{Equation 2-3}$$

Thus

$$u_{ab} = R(i_a - i_b) + L\frac{d}{dt}(i_a - i_b) + e_a - e_b \qquad \textbf{Equation 2-4}$$

$$u_{bc} = R(i_b - i_c) + L\frac{d}{dt}(i_b - i_c) + e_b - e_c \qquad \textbf{Equation 2-5}$$

$$u_{ca} = R(i_c - i_a) + L\frac{d}{dt}(i_c - i_a) + e_c - e_a \qquad \textbf{Equation 2-6}$$

Where

R: Armature resistance

L_s: Armature inductance

M: Mutual inductance, which describes the flux linkage between two windings

$e_{a,b,c}$: The Back-EMF

$i_{a,b,c}$: The armature currents flowing through windings

$u_{a,b,b}$: The phase voltages

u_{ab},u_{bc} and u_{ca}: The phase-to-phase voltages

The relationship between phase currents is given by the Equation 2-7:

$$i_a + i_b + i_c = 0 \qquad \textbf{Equation 2-7}$$

Since each voltage is a linear combination of the other two voltages, two equations are sufficient. By neglecting one equation and eliminating one variable using Equation 2-7, Equation 2-4 and Equation 2-5 can be written as:

$$u_{ab} = R(i_a - i_b) + L\frac{d}{dt}(i_a - i_b) + e_a - e_b \qquad \textbf{Equation 2-8}$$

$$u_{bc} = R(i_a + 2i_b) + L\frac{d}{dt}(i_a + 2i_b) + e_b - e_c \qquad \textbf{Equation 2-9}$$

From the Newton's second law of motion, the relation between electromagnetic torque T_e and speed of motor ω_m can be written as following:

$$T_e - T_l = J\frac{d\omega_m}{dt} + B\omega_m \qquad \textbf{Equation 2-10}$$

$$\omega_m = \frac{d\theta_m}{dt} \qquad \textbf{Equation 2-11}$$

Where

T_l: Load torque in Nm

J: Moment of inertia in kg/m^2

B: Damping constant

The Back-EMF and electromagnetic torque can be expressed as

$$e_a = \frac{k_e}{2}\omega_m F(\theta_e) \quad \textbf{Equation 2-12}$$

$$e_b = \frac{k_e}{2}\omega_m F(\theta_e - \frac{2\pi}{3}) \quad \textbf{Equation 2-13}$$

$$e_c = \frac{k_e}{2}\omega_m F(\theta_e - \frac{4\pi}{3}) \quad \textbf{Equation 2-14}$$

$$T_a = \frac{k_t}{2} i_a F(\theta_e) \quad \textbf{Equation 2-15}$$

$$T_b = \frac{k_t}{2} i_b F\left(\theta_e - \frac{2\pi}{3}\right) \quad \textbf{Equation 2-16}$$

$$T_c = \frac{k_t}{2} i_c F(\theta_e - \frac{4\pi}{3}) \quad \textbf{Equation 2-17}$$

Thus

$$T_e = \frac{k_t}{2}[F(\theta_e) i_a + F\left(\theta_e - \frac{2\pi}{3}\right) i_b + F(\theta_e - \frac{4\pi}{3}) i_c] \quad \textbf{Equation 2-18}$$

Where k_e and k_t are Back-EMF constant and electromagnetic torque constant respectively. The electrical angle θ_e is equal to the mechanical angle θ_m of motor multiplied by number of pole pairs ($\theta_e = \frac{p}{2}\theta_m$). The function $F(\theta)$ is a function of rotor position, which gives the trapezoidal waveform of Back-EMF. One period of function can be given as:

$$F(\theta_e) = \begin{cases} 1, & 0 \le \theta_e < \frac{2\pi}{3} \\ 1 - \frac{6}{\pi}\left(\theta_e - \frac{2\pi}{3}\right), & \frac{2\pi}{3} \le \theta_e < \pi \\ -1, & \pi \le \theta_e < \frac{5\pi}{3} \\ 1 + \frac{6}{\pi}\left(\theta_e - \frac{2\pi}{3}\right) & \frac{5\pi}{3} \le \theta_e < 2\pi \end{cases}$$

Equation 2-19

Due to the symmetry design of motor, the Back-EMF signal of each phase is 120 degrees phase shifted with respect to each other as shown in Figure 2-5.

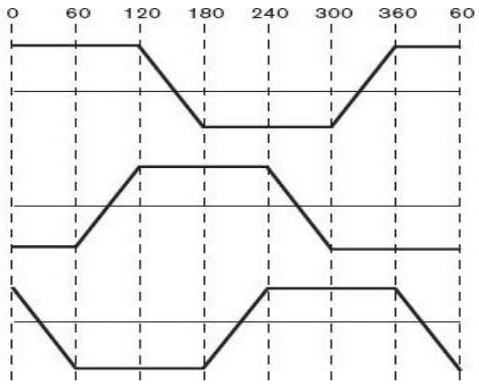

Figure 2-5 Back-EMF signals with 120 degrees phase shift

3. Electrical Commutation System

In order to drive a BLDC motor, an electronic circuit implementing the electrical commutation is required. To do so, firstly it is needed to come up with a way to drive the motor based on a predefined sequence lookup table which is made up with different position states of the rotor. In this project, a two-level three-phase full-bridge MOSFET inverter is exploited to implement the power switching function. It is also integrated with some other circuitries which get the position information, process it and then deliver the gate drive signals in order to switch the inverter transistors. In following, we are going to discuss each part briefly.

3.1. Inverter

In definition, an Inverter is a device designed to convert DC power to AC power [7]. As the power inverters are constructed by power electronic switches, their output is in a discrete form made by fast state transition of transistors [3]. Figure 3-1 shows a three-phase full-bridge inverter consisting of three legs which each functions for an individual phase. Each of the two switches in each leg is determining either the positive or the negative half of the DC link is conducted to the output. By switching the transistors complementarily in each leg, the current flows through the transistor which conducts positive end of the DC link and returns back through another transistor in other two legs which are conducting the negative end.

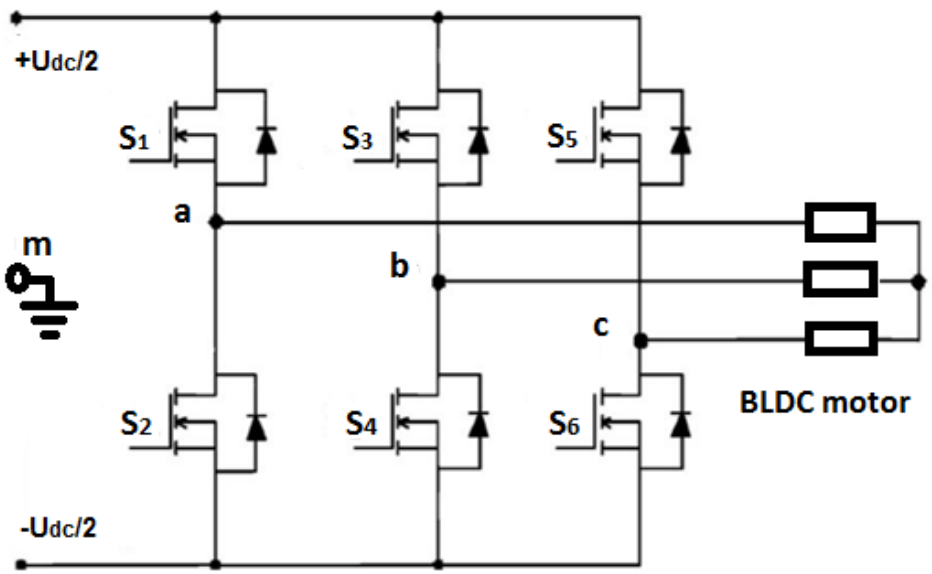

Figure 3-1 Three-phase inverter

Consider the DC link voltage split into two halves with the midpoint[1] 'm'; Then the voltage of each leg midpoint is represented by u_{am}, u_{bm} and u_{cm}. Respectively, the Line-to-Line voltages are derived by midpoint voltages as follow:

$$u_{ab} = u_{am} - u_{bm} \qquad \textbf{Equation 3-1}$$

$$u_{bc} = u_{bm} - u_{cm} \qquad \textbf{Equation 3-2}$$

$$u_{ca} = u_{cm} - u_{am} \qquad \textbf{Equation 3-3}$$

Based on switching signals S_1 to S_6, the respective transistor switches ON or OFF and produce output signals. In this Project, these switching signals are a combination of modulated reference from controllers and commutation sequences based on Hall Effect Sensors data.

In following, the Pulse Width Modulation will be discussed briefly then it will be explained how these PWM signals are combined to the commutation sequences.

3.2. Pulse Width Modulation (PWM)

The Pulse Width Modulation is a modulation technique that adjusts the duty cycle of a pulse with respect to the modulator signal information. This technique enables us to control the electrical power applied to analog circuits such as electric motors based on the information from controllers. As mostly all digital processors are equipped with PWM, this has turned out to be one of the most popular control approaches [8] [9].

Considering the signal from controllers as a continuous value

$$s^* \in [-1, +1], \qquad \textbf{Equation 3-4}$$

the PWM approximates this value by a discrete-value function

$$s_{(t)} \in [-1, +1], \qquad \textbf{Equation 3-5}$$

so that the average value within the switching period T_s is equal to the desired value shown as follow:

[1] It does not exist physically and is introduced only for the sake of clarification in explanation.

$$\bar{s} = \frac{1}{T_s} \int_{kT_s}^{(k+1)T_s} s_{(t)} dt = s^* \qquad \textbf{Equation 3-6}$$

where one can compute the actual desired value as follow [10]:

$$u^* = s^* \, U_d \qquad \textbf{Equation 3-7}$$

The simplest way to generate a PWM signal is to compare the reference signal[2] with a triangular or a sawtooth waveform by a comparator such that when the value of the reference signal grows greater than modulation waveform, the PWM gets the high state otherwise it stays in the low state [8]. Figure 3-2, illustrates the PWM generation with triangular modulation waveform and a constant reference signal.

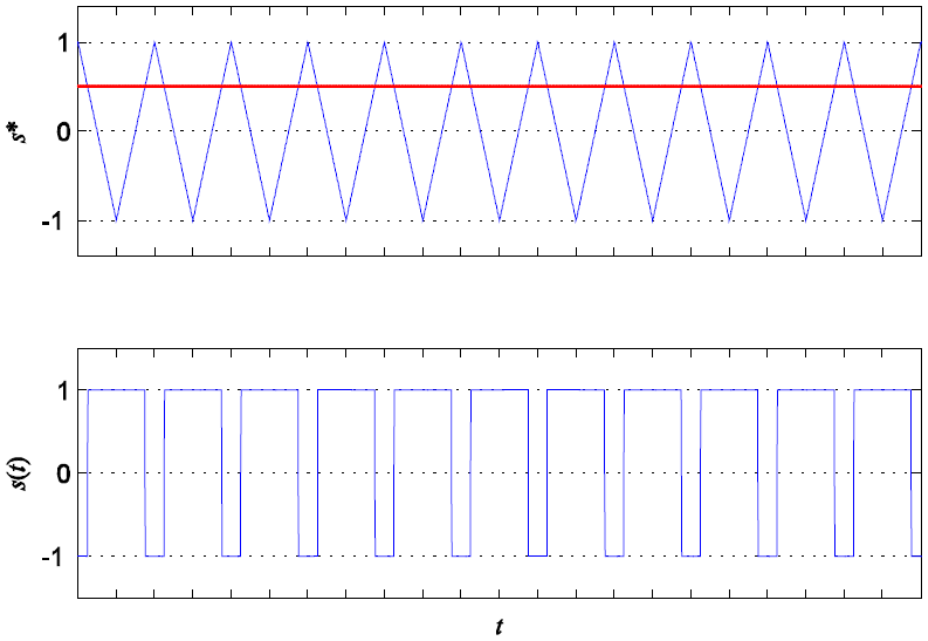

Figure 3-2 Principle of pulse width modulation [10]

The whole mechanism can be simply illustrated in Figure 3-3.

[2] The signal which is given by the controller.

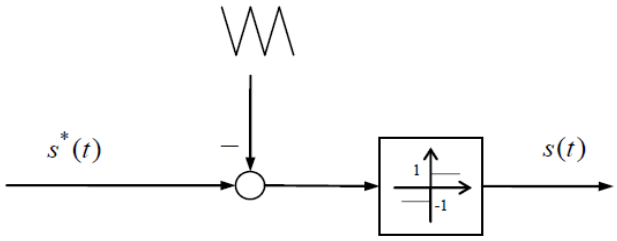

Figure 3-3 Realization of the pulse width modulation by triangular modulation carrier and a comparator. [10]

3.3. Commutation

In order to drive a BLDC motor, it is required to know about the actual position of the rotor. In some types of BLDC motors, three hall-effect sensors are employed with 120-degree intervals on the stator. By rotating of the rotor, they produce three distinct signals with 120 degrees phase difference and 180 degrees length. Each sensor has a rising and falling edge when the magnet poles of the rotor come to the sensors [11]. The Back EMF and hall-effect signals are presented in Figure 3-4.

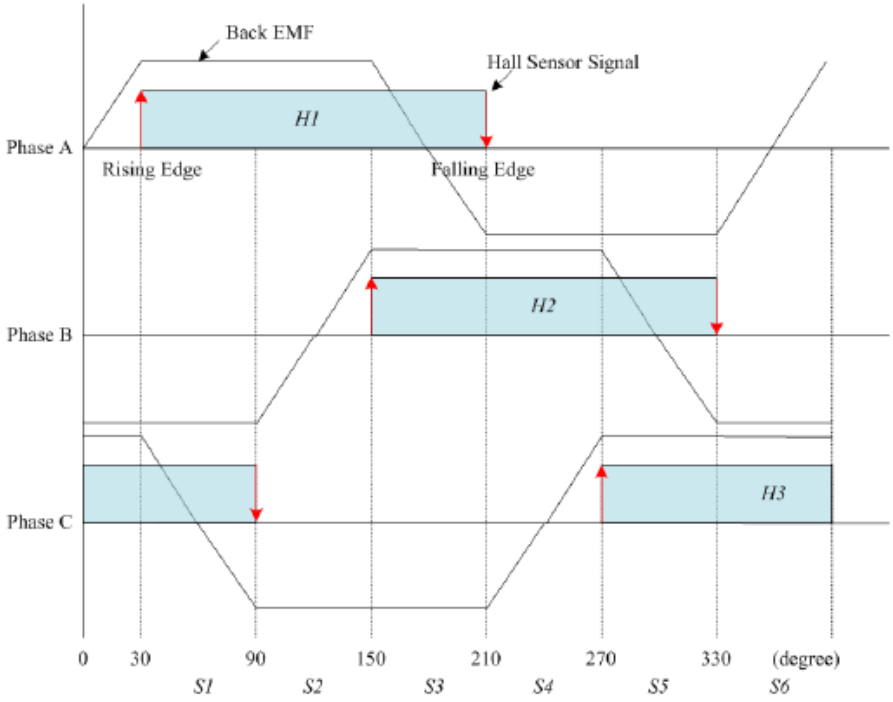

Figure 3-4 Back EMF and hall-effect sensor signals [11]

As shown in Figure 3-4, the common operation of a BLDC motor is fulfilled in six steps. The timing of both signals gives a hint to build up a sequence lookup table of conducting pair phases for each distinct

step. The switching sequences required for the inverter can be extracted from the lookup table presented in Table 3-1. The current in each phase is blocked for 60 degrees after a 120-degree interval of conduction as it is implemented in Table 3-1; by knowing the fact that the Back-EMF has the maximum value when the current is flowing through the corresponding phase.

Seq.	H1	H2	H3	Phase a	Phase b	Phase c
1	1	0	1	$+\frac{U_{dc}}{2}$	$-\frac{U_{dc}}{2}$	NC
2	1	0	0	$+\frac{U_{dc}}{2}$	NC	$-\frac{U_{dc}}{2}$
3	1	1	0	NC	$+\frac{U_{dc}}{2}$	$-\frac{U_{dc}}{2}$
4	0	1	0	$-\frac{U_{dc}}{2}$	$+\frac{U_{dc}}{2}$	NC
5	0	1	1	$-\frac{U_{dc}}{2}$	NC	$+\frac{U_{dc}}{2}$
6	0	0	1	NC	$-\frac{U_{dc}}{2}$	$+\frac{U_{dc}}{2}$

Table 3-1 Commutation sequence for clockwise rotation

Prior to applying such gate-drive signals, one should come up with a way to combine them with the PWM signal. It means that each gate-drive signals based on hall-effect signals are switched by a higher-frequency PWM signal. By doing that, we are able to control the voltage applied to the motor by changing the PWM duty cycle. More detail will be given in following sections.

4. SIMULINK/MATLAB Models

In this section, the SIMULINK/MATLAB implementation of the BLDC motor drive model is presented. Figure 4-1 shows the contents of the complete BLDC motor drive. The PLECS tools are used to implement the BLDC motor integrated with surround sub-blocks, in order to build up the complete drive model. PELCS is a simulation platform for power electronic systems, which offers wide range of built-in components that make modeling easier. In the following sub-sections, the functionality of individual sub-blocks will be described.

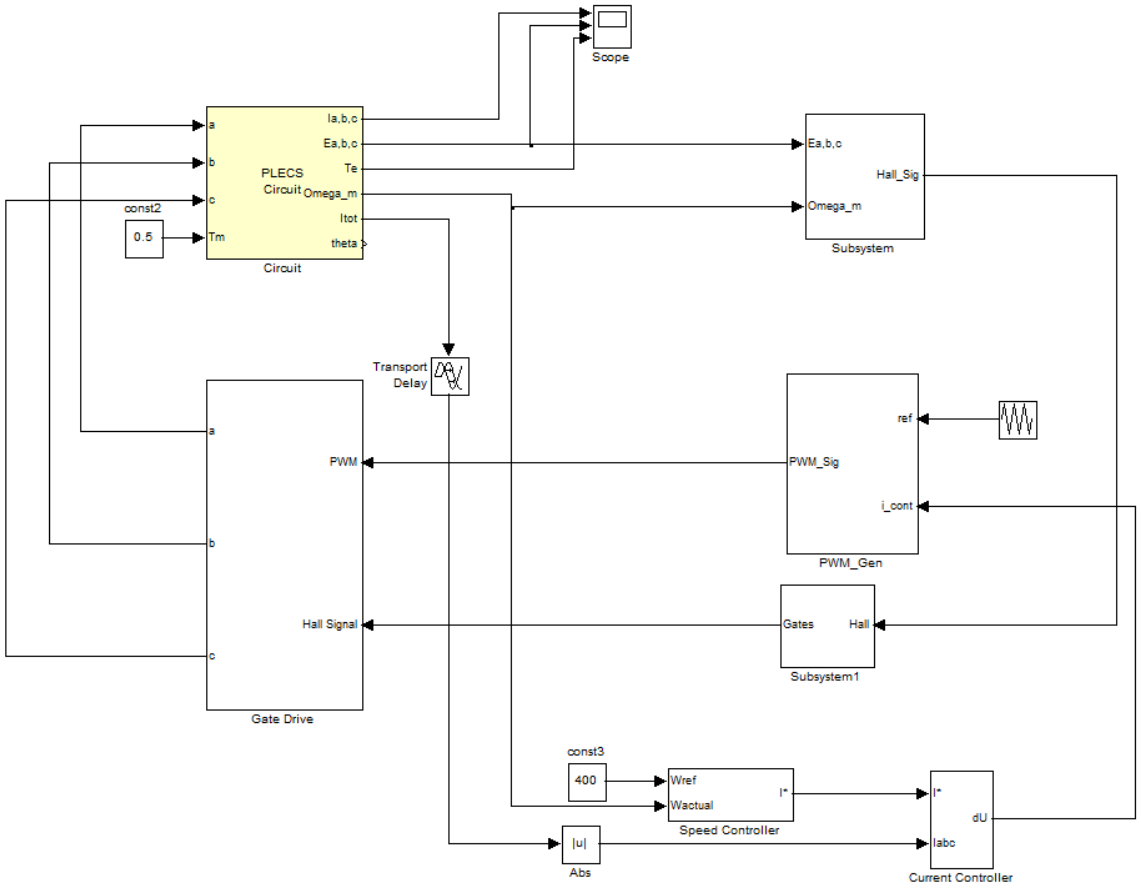

Figure 4-1 Complete electric drive of a BLDC motor

4.1. PLECS Three-phase BLDC Motor Model

The following data and parameters of the motor have been taken from the datasheet of the BLDC motor (*ME0201013001*) by "Mars Electric LLC" company and previous work [12]:

Supplied DC voltage: 24-48 V

Maximum current: 300 A

Line to line winding resistance: 13 mΩ

Line to line winding inductance: 60 µH

Poles Number: 4

Torque constant K_t: 0.1364 Nm/A

Back-EMF constant K_e: 0.0325 Vs

The three-phase BLDC motor model in PLECS is shown in Figure 4-2, which basically contains two main Parts namely the Back-EMF and the mechanical system and will be explained respectively.

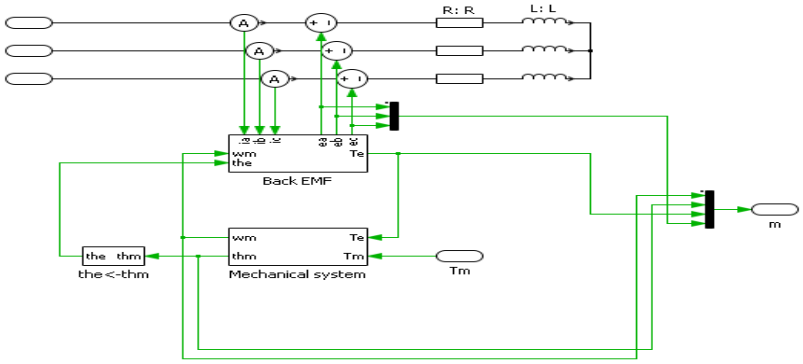

Figure 4-2 Three-phase BLDC motor PLEC model

The Back-EMF block is used to model the Back-EMF signals and the electrical torque. In this block, armature currents and the electrical angle are taken as inputs while the electrical torque and the Back-EMF signals are as outputs. The Figure 4-3 shows the detailed Back-EMF block, where the Equation 2-4 to Equation 2-6 are employed to drive the armature currents $i_{a,b,c}$ and the Equation 2-12 to Equation 2-18 are used to model Back-EMF signals and electrical torque respectively. In addition, in this model, the electrical torque and Back-EMF constant are assumed equal in case that they are expressed in volt-sec/rad for a constant-flux machine [13].

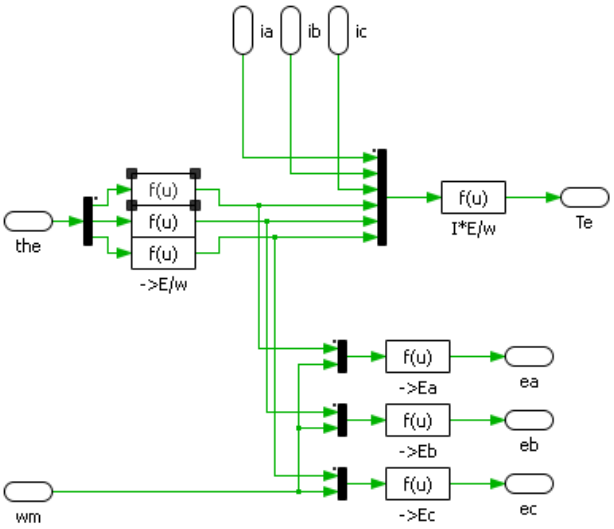

Figure 4-3 Back-EMF block

In the following, the mechanical system is described. It takes the electrical and load torque[3] as inputs and gives mechanical speed (motor speed) as the output. The mechanical system model is based mainly on the Equation 2-10 and Equation 2-11. After taking the integration of mechanical speed ω_m, the mechanical angle is calculated, which is used to compute the electrical angle considering the relationship[4] between them. The computed electrical angle is also required in order to model the Back-EMF block. The detailed mechanical system is shown in Figure 4-4.

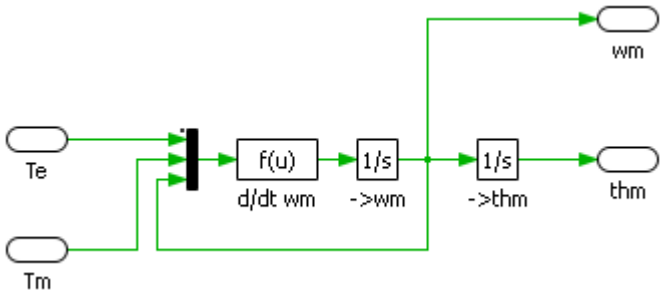

Figure 4-4 Mechanical system

4.2. Hall-effect Sensors Block

As discussed in part 3.3, the hall-effect signals can be extracted from the Back EMF signals. Therefore, to model the sensors signals, we need to manipulate the Back EMF signals provided by the motor block. Having a glance at the Back EMF equation, we can see that it is proportional to rotational

[3] The load torque is assumed constant.

[4] $\theta_e = \frac{p}{2}\,\theta_m$

speed ω_m. In order to obtain the hall-effect signals, its effect should be excluded. Therefore, the Back-EMF signals are normalized by rotational speed so the instantaneous values are independent from the speed. The block construction is presented in Figure 4-5.

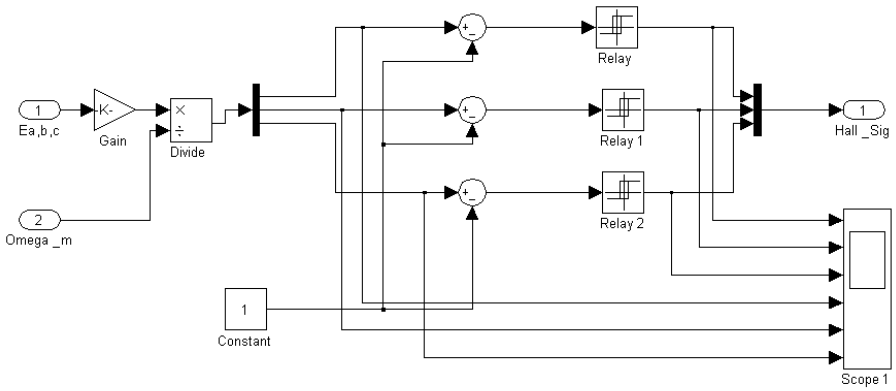

Figure 4-5 Hall-effect signals block

4.3. Gate Signal Generator Block

This Block is designed to generate gate signals based on the lookup Table 3-1 in which $+\frac{U_{dc}}{2}$ means the upper transistor and $-\frac{U_{dc}}{2}$ means the lower transistor in respective leg is conducting. It gets three hall signals as inputs and after processing them, delivers six gate signals which are intended to switch the inverter MOSFETs. In this model, the AND-OR gate logics are used to build up the lookup table. Figure 4-6 shows the relationship between gate signals, hall-effect and Back-EMF signals for phase a.

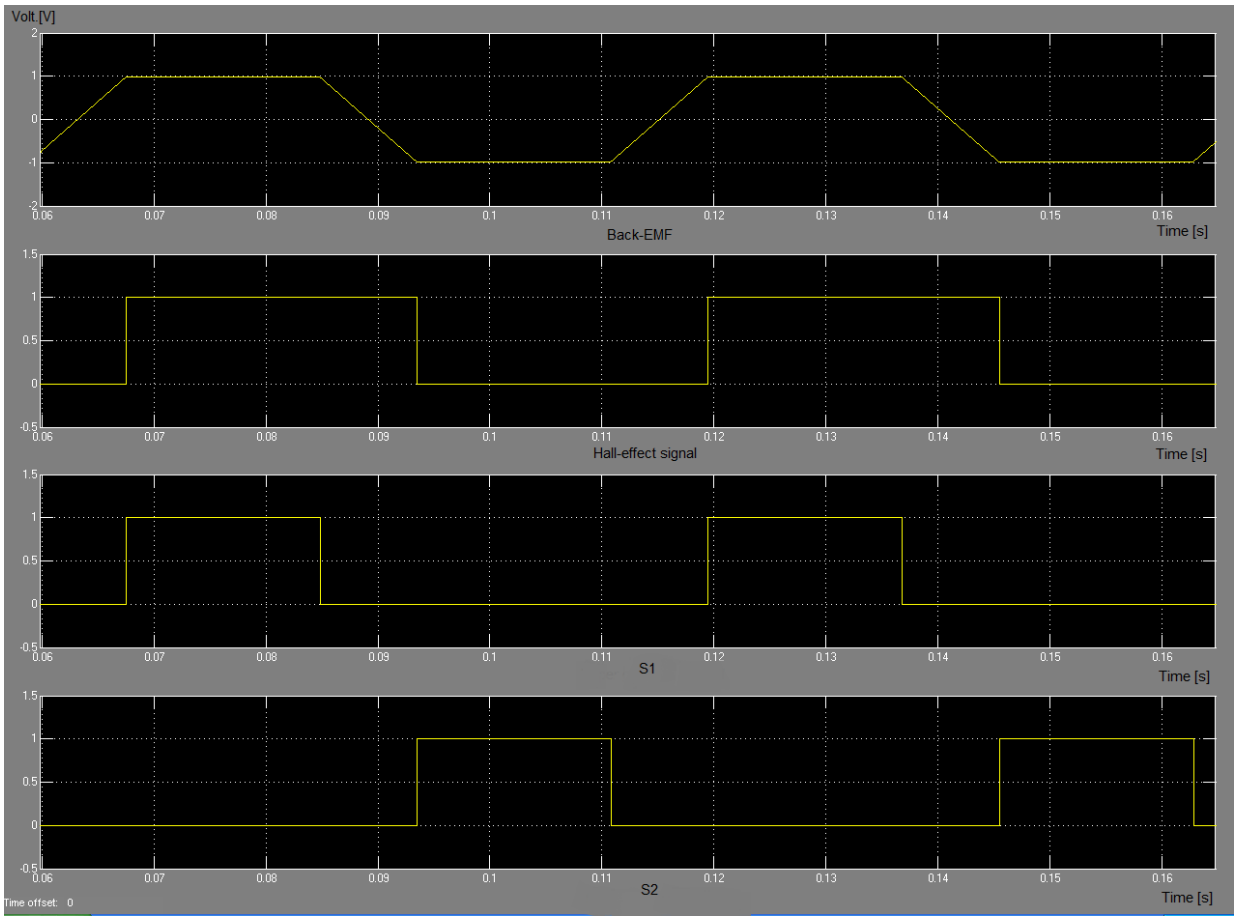

Figure 4-6 The relationship between the Back-EMF, the hall-effect signal and the gate signals for phase a
This relationship holds for other two phases considering that they are 120 degrees shifted to each other..

4.4. Pulse Width Modulation Block

This block implements a simple method to generate PWM signal. As discussed in 3.2, a triangular waveform is compared with a reference value coming from controller blocks and the result will be saturated to zero or one in case it is either a positive or negative value. The obtained output is totally the same as Figure 3-2. The model block is presented in Figure 4-7.

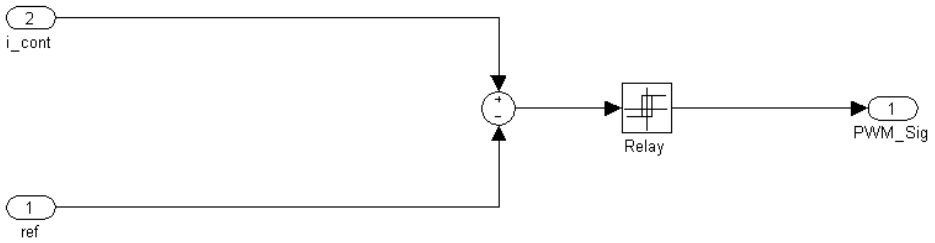

Figure 4-7 Pulse width modulation block

4.5. Gate Drive Block

Merging the PWM and Gate signals are done by this block. These two signals are given to the input and three commutation signals which are switched with the same frequency as the PWM signal are delivered to the output of this block. Each output contains gate drive signals of the respective phase where the positive and negative halves of the signal are switching the upper and lower transistors respectively. The block configuration is shown in Figure 4-8. The resulting output is illustrated in Figure 4-9.

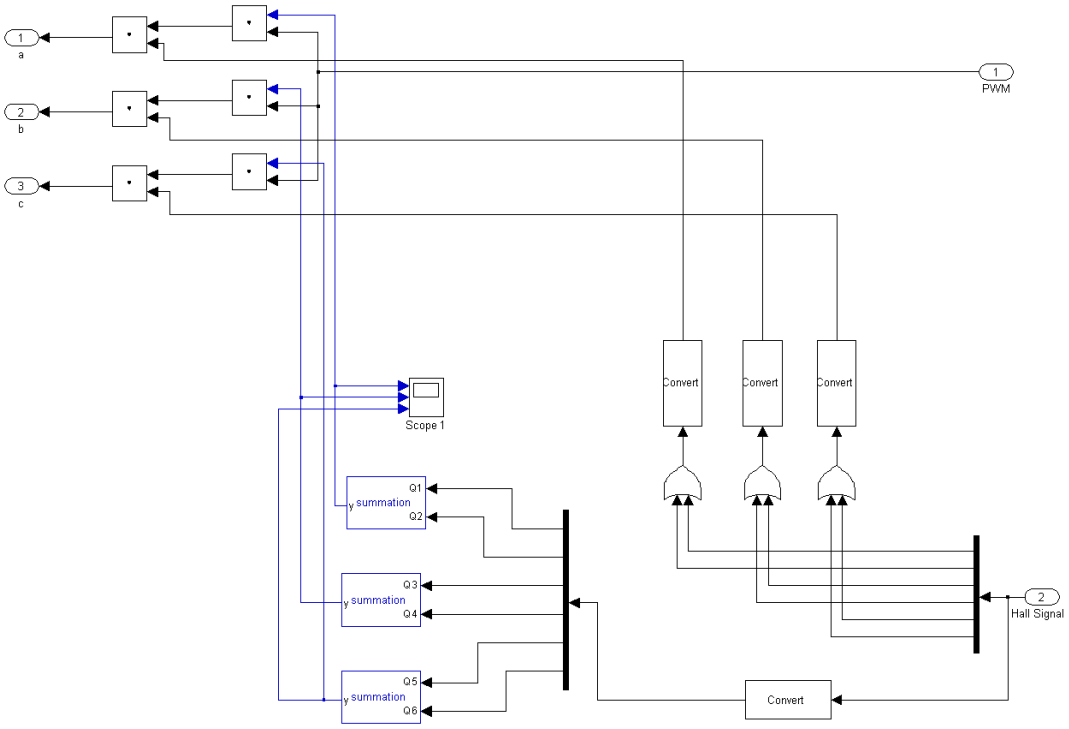

Figure 4-8 Gate drive Block which combines the PWM and gate signals

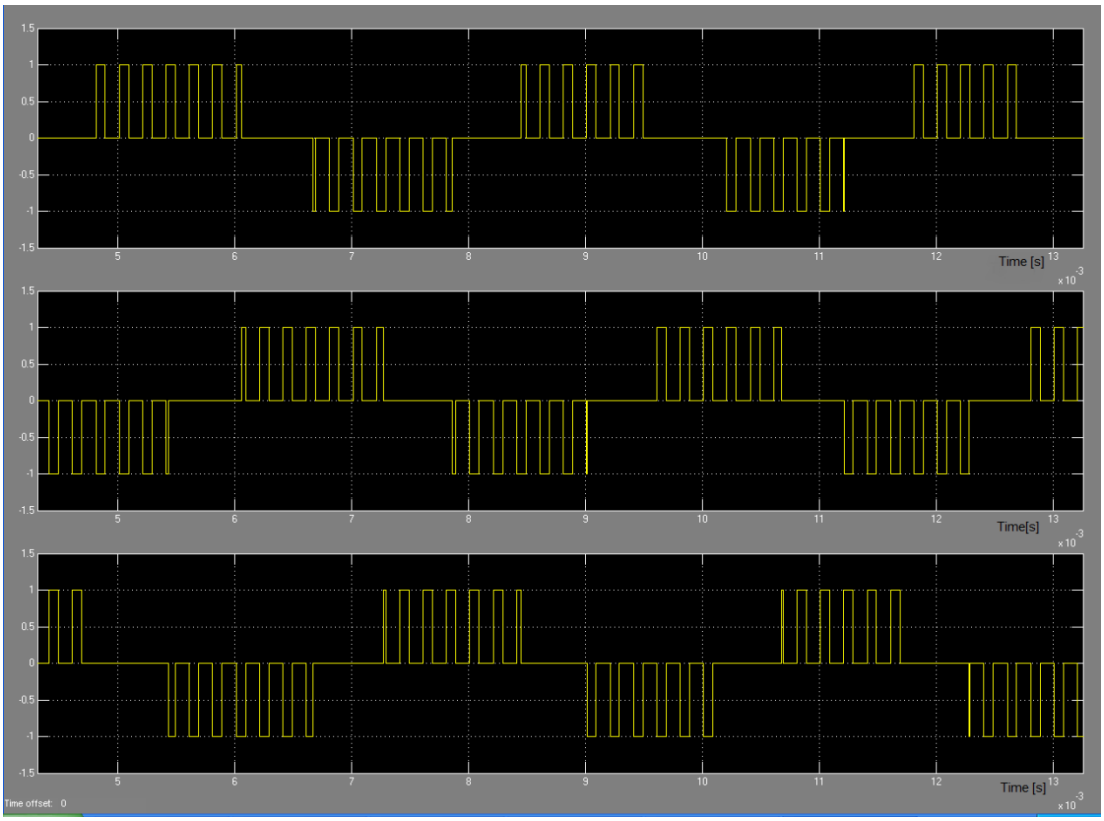

Figure 4-9 Gate drive signals

4.6. Inverter

The predesigned two-level MOSFET inverter in PLECS toolbox is used in this model. In this block, the gate drive signals and DC link voltage is given as input and three line voltages are delivered to the motor. The configuration of the inverter and the motor is presented in Figure 4-10.

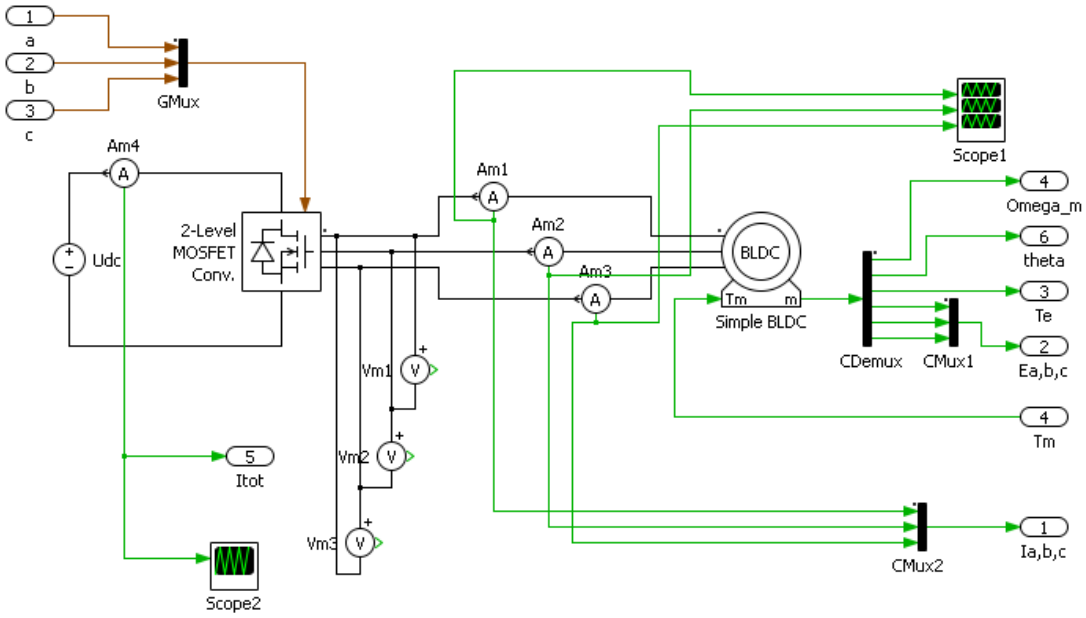

Figure 4-10 The configuration of inverter and motor in PLECS environment

5. Proposed Control Method

Since the work is meant for electric hybrid vehicle, the main concern turns out to be to control the speed. Due to the fact that the current may exceed the maximum rating of the motor, a current controller is also introduced in order to maintain it below a limit. The anti-windup control method is used in order to improve the response of the system

The control structure of the motor is illustrated in Figure 5-1. As can be seen, the needed torque T^* required to achieve the desired given speed is generated by a speed controller. The proportional current i^* to this torque is limited by the maximum current of the motor before being applied to the current controller. This guarantees that the current will be maintained in the motor range. A time constant τ_σ is also considered which refers to delays appearing in the system due to sensors, switching circuitry and control implementation.

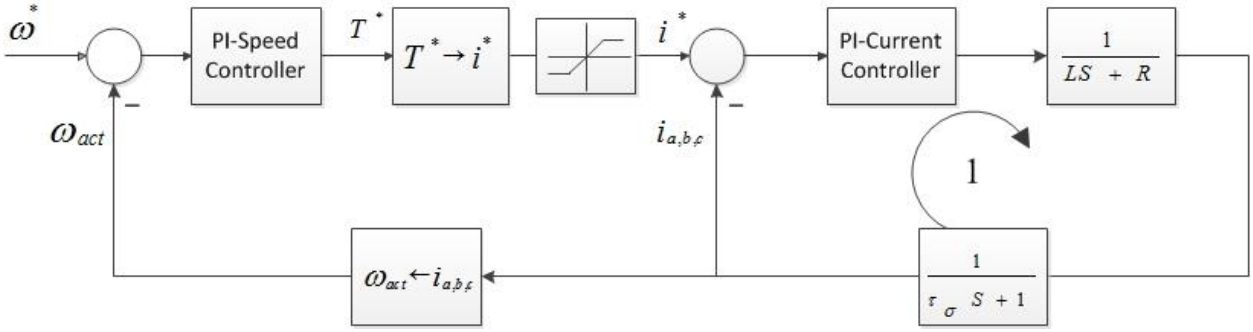

Figure 5-1: Block Diagram describing the system

5.1. The PI-Current Controller

The current controller is of a PI type as shown in Figure 5-2. The controller gains and time constant are calculated based on the pole-zero cancelation design method. Given $L_s = 30\ \mu H$ and $R_s = 6.5\ m\Omega$ be the electrical characteristic of the motor and $\tau_\sigma = 0.25\ \mu s$ the delay time constant, the loop transfer function is obtained as follows.

$$L(s) = V_s V_c \frac{1}{1+\tau_s} \frac{1}{1+\tau_\sigma} \frac{1+sT_n}{sT_n} \qquad \text{Equation 5-1}$$

where τ_s is the motor time constant and equals $\frac{L_s}{R_s}$ and V_s equals $\frac{1}{R_s}$. The controller parameters used in Equation 5-1 are also defined after some reconfiguration in the basic equation:

$$G_c(s) = K_p + \frac{K_i}{s} = K_p \frac{1 + s\frac{K_p}{K_i}}{s\frac{K_p}{K_i}} = V_c \frac{1 + sT_n}{sT_n} \qquad \text{Equation 5-2}$$

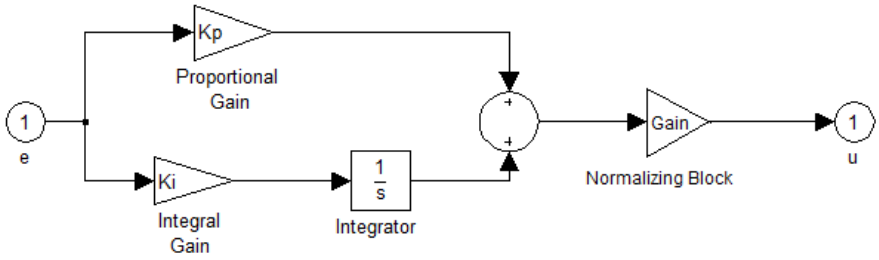

Figure 5-2 PI-current controller

The pole-zero cancelation method results in $K_p = 30$ and $K_i = 6.5 \times 10^3$ then $T_n = 4.615\, ms$. As shown on the bode diagram plotted based on calculated control parameters (Figure 5-3), the resulted phase margin is sufficiently 76 degrees which verifies the stability of the controller and the design accuracy.

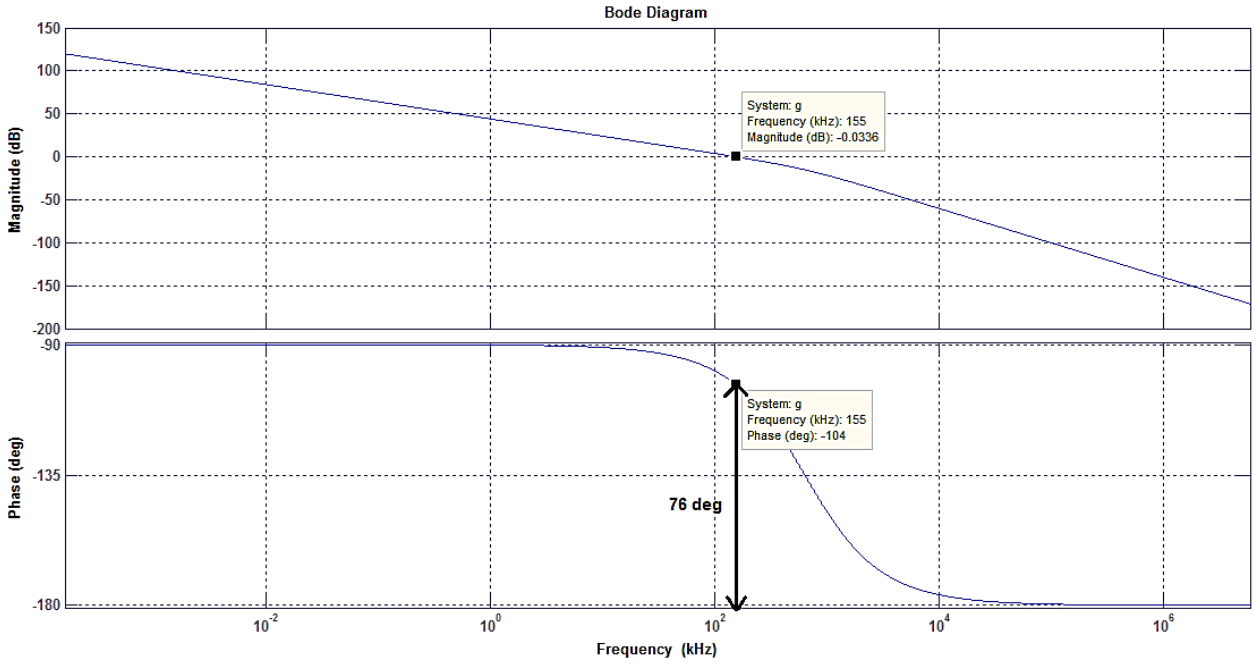

Figure 5-3The bode diagram for loop tranfer function of current controller

5.2. The PI-Speed Controller

A PI-type controller is also employed for speed controller as shown in Figure 5-4. The symmetrical optimum method is used to design the controller. The control parameters are calculated with respect to the results obtained in the current controller. The detailed design strategy is explained thoroughly in [10].

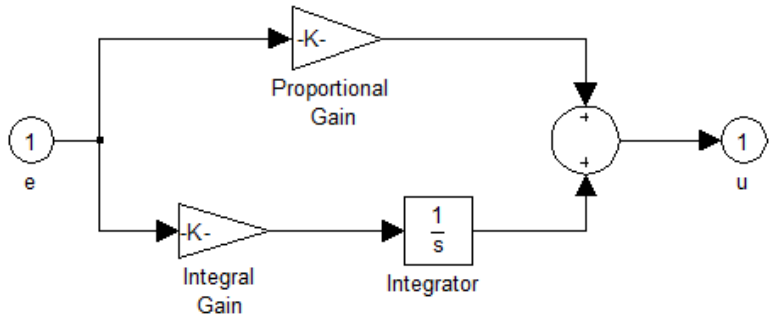

Figure 5-4: PI-Speed Controller

Given the previous results from the current controller design, the symmetrical optimum design method delivers $K_{p-s} = 28.84 \times 10^3$ and $K_{i-s} = 5.76 \times 10^7$ as control parameters of the speed controller. Figure 5-5 shows the bode diagram plotted for the loop transfer function of the speed controller (the outer loop of control structure). As it shows, the phase margin has a sufficiently high value of 76 degrees.

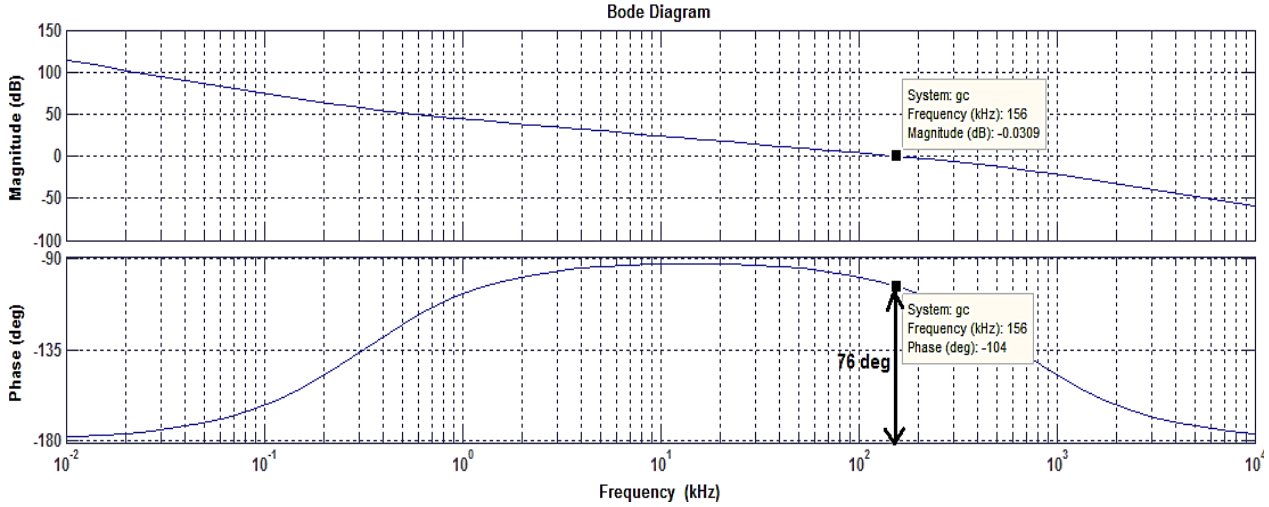

Figure 5-5 The bode diagram for the speed controller

6. Results

Figure 6-1 illustrates the response of the system to the given value of ω_m^*. As can be seen, the motor speed settles by the given speed after approximately 90ms with a negligible overshoot. More details can be seen in a zoomed version of the response in Figure 6-2, where it plateaus to the steady state value

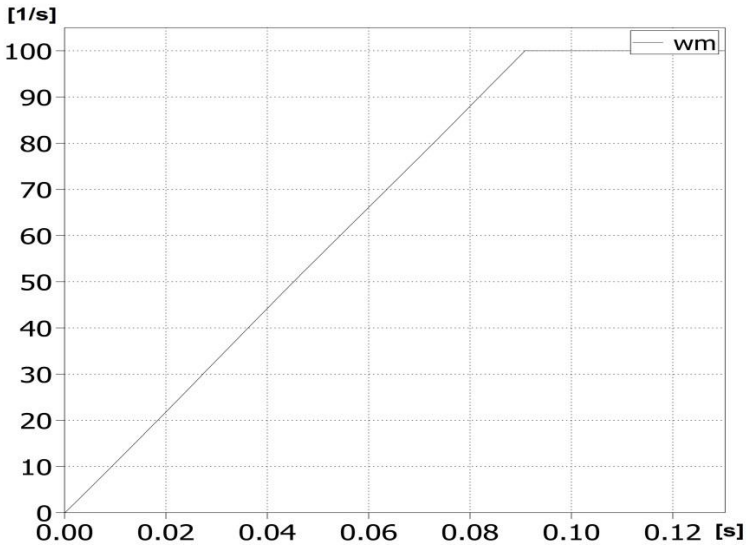

Figure 6-1 the motor rotational speed for $\omega_m^* = 100s^{-1}$ and $J = 0.0052\ Nms^2$

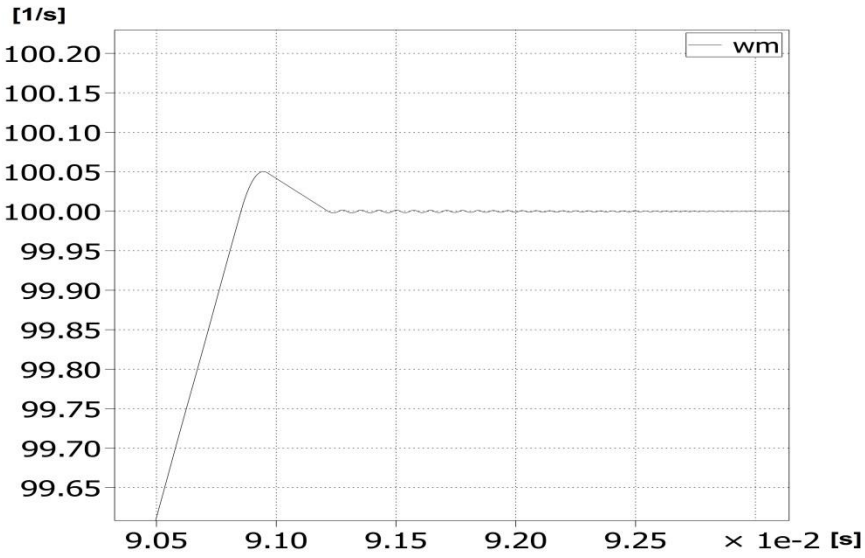

Figure 6-2 A zoomed version of Figure 6-1 on the overshooting period

Once a desired speed is applied to the speed controller, a high amount of electrical torque is generated regarding the load and difference between the desired and actual speed. This high torque remains until the motor speed reaches the desired value (i.e. the changing rate of speed becomes zero). This implies that the electrical toque T_e drops to a value equal to the mechanical (load) toque T_L based on the Equation 2-10.

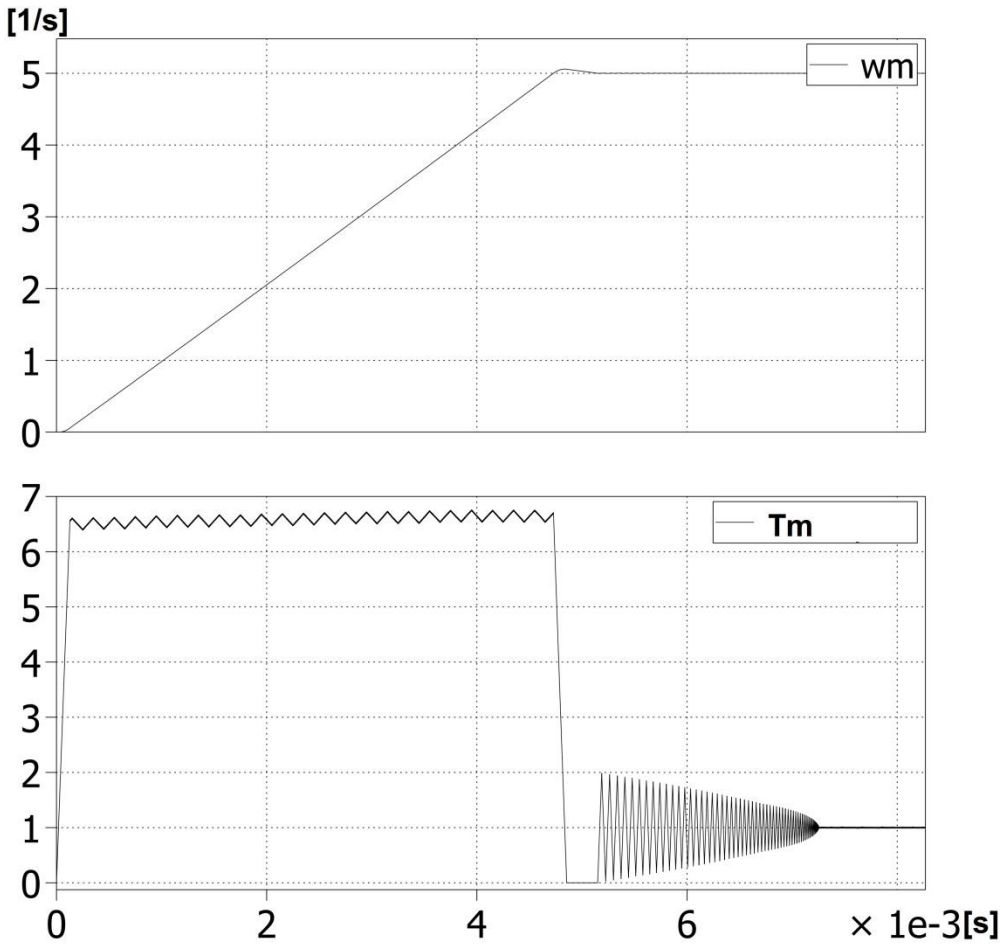

Figure 6-3 The changes of the electrical torque with changing of motor speed for $T_e = 1\ Nm$, $J = 0.0052\ Nms^2$ and $\omega_m^* = 5\ s^{-1}$

The current applied to the current controller is proportional to the torque generated by the speed controller. However, it is limited by the maximum current of the motor earlier. Figure 6-4 shows the current in transient and steady-state for phase *c*. The spikes on each pick are happening at the switching events.

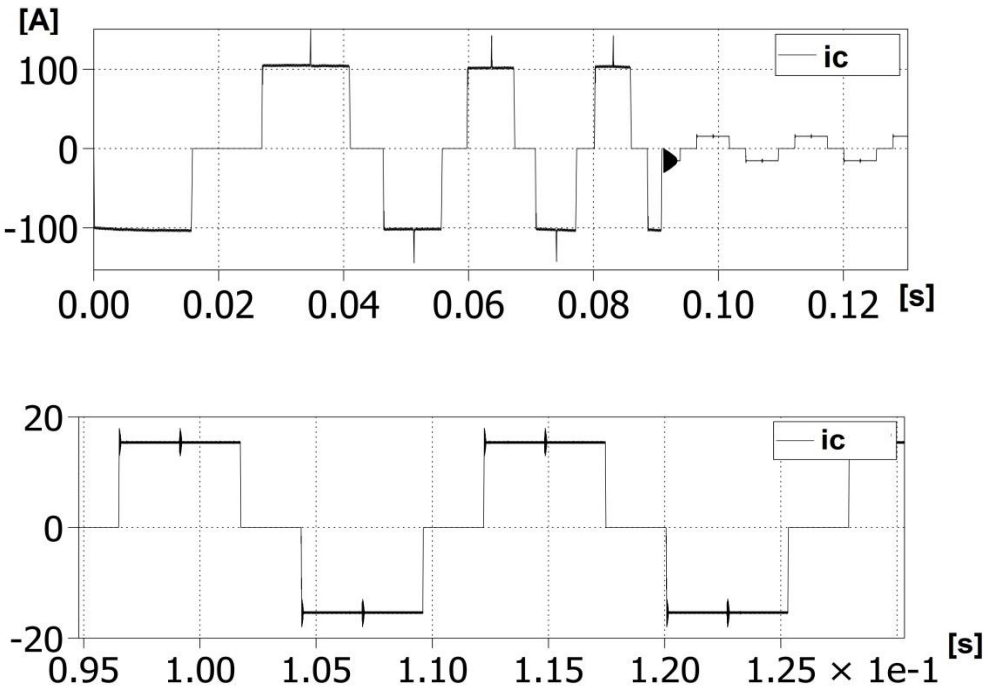

Figure 6-4 Phase current of the motor in the transient and the steady-state speed for phase c (other phase currents are shifted by 120 degress)

The control system is also tested against the changes in load while the motor is running with a specific speed. The result in Figure 6-5 shows that the motor maintains the speed after the changing of the load from 1Nm to 1.2 Nm. As can be noticed in the figure, a damping fluctuation in speed is happening at the time of the torque change due to the dynamic behavior of the system. However, the speed settles down on the given speed again after a very short time. This control feature demonstrates its importance when the vehicle is running on a slope-varying road.

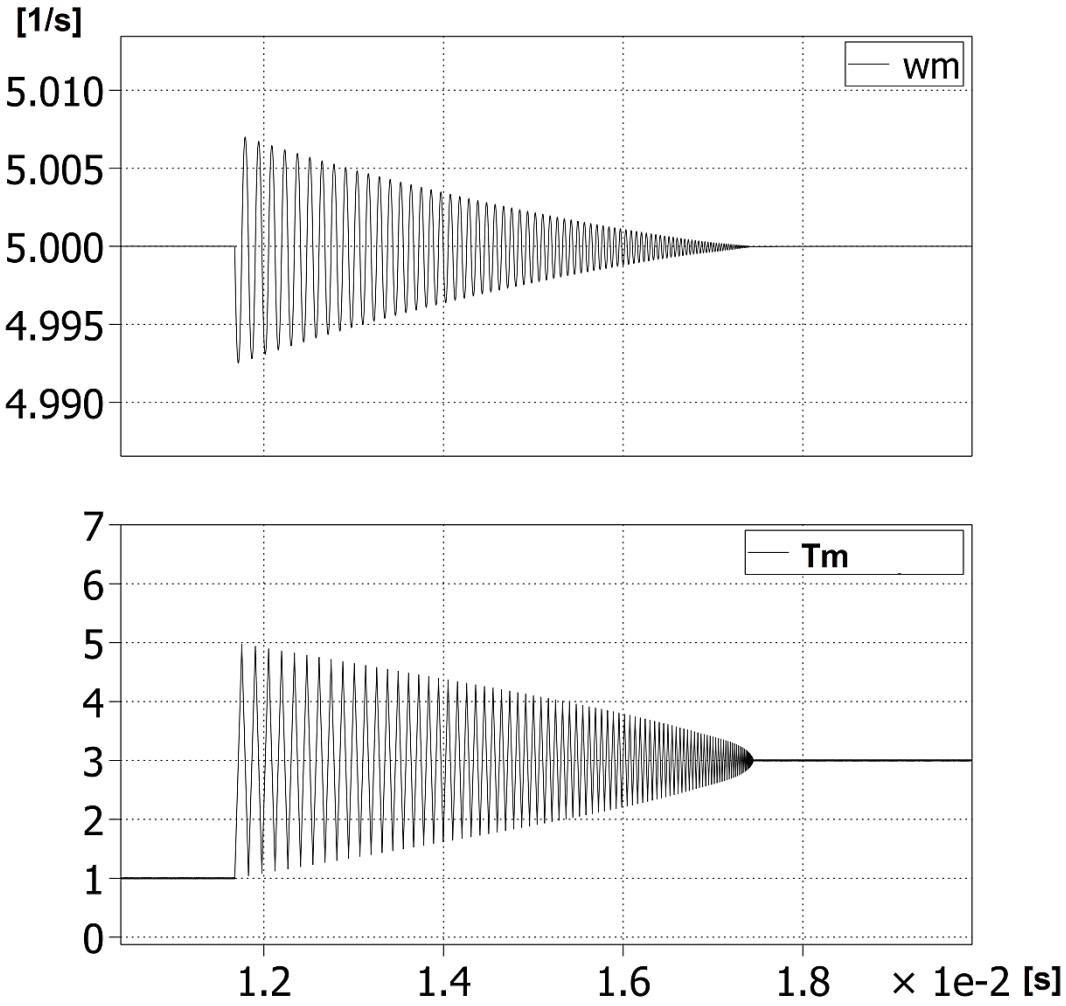

Figure 6-5 The motor speed against changing of load from 1 Nm to 3 Nm

7. Conclusion

In this report, the modeling and simulation of the BLDC motor drive system is presented. The model is developed in SIMULINK/MATLAB using PLEC toolbox. By employing the PI-current and –speed controllers, the motor is able to follow the desired speed. Furthermore, the motor current is controlled below a maximum limit. The motor is also able to maintain its speed against the load variation.

For future works, some other parameters such as inverter dead-time can be considered. It is also recommended to develop the breaking control mode to provide the motor speed control in reducing speeds.

8. Bibliography

[1] Microsemi Corporation, "Speed Control of Brushless DC Motors-Sinusoidal Commutation with Hall," Microsemi Corporate Headquarters, Aliso Viejo CA, 2012.

[2] J. S. B. G. M.V.Ramesh., "Speed Torque characteristics of Brushless DC motor in either direction on load using ARM controller," *Journal of Energy Technologies and Policy*, vol. 2, 2011.

[3] M. P. Kazmierkowski, M. Malinowski and M. Bech, "Pulse Width Modulation Techniques for Three-Phase Voltage Source Converters," in *Control in Power Electronics*, M. P. Kazmierkowski, R. Krishnan and F. Blaabjerg, Eds., Warsaw, Aalburg, Academic Press, 2002, pp. 89-160.

[4] J. W. Dixon and I. A. Leal, "Current Control Strategy for Brushless DC Motors," *IEEE TRANSACTIONS ON POWER ELECTRONICS*, vol. 17, pp. 232-240, march 2002.

[5] A. Vinod KR Singh Patel., "Modeling and Performance Analysis of PID Controlled BLDC Motor and Different Schemes of PWM Controlled BLDC Motor," *International Journal of Scientific and Research Publications*, vol. 3, no. 4, pp. 1-14, April 2013.

[6] D. C. Hanselman, Brushless Permanent Magnet Motor Design, 2 ed., Magna Physics Publishing, 2006.

[7] D. Ton, A. Bulawka and W. Bower, "Summery Report on the DOE Workshop on a System-Driven Aproach to Inverter Research and Development," Washington DC; Albuquerque, 2003.

[8] Wikipedia, 6 November 2013. [Online]. Available: http://en.wikipedia.org/wiki/Pulse-width_modulation. [Accessed 12 11 2013].

[9] M. Barr, 07 November 2007. [Online]. Available: http://www.barrgroup.com. [Accessed 12 November 2013].

[10] J. Boecker, *Mechatronics and Electrical Drives, Lecture Script,* Paderborn: University of Paderborn, 2012.

[11] S. Y. Yun, H. J. Lee, J. H. Han and J. Lee, "Position Control of Low Cost Brushless DC Motor Using Hall Sensor," *Electromagnetic Field Problems and Applications (ICEF), 2012 Sixth International Conference on* , pp. 19-21, June 2012.

[12] B. R. K. T. T. W. A. K. L. Schlenger A., "Projektseminar WS 2012/2013 ,Mechatronik/Elektrische Antriebe," Paderborn, 2013.

[13] R. Krishnan, elctrical motor drives: modeling, analysis, and control, prentice hall, 2001.

[14] V. Fedak, T. Balogh and P. Zaskalicky, "Dynamic Simulation of Electrical Machines and Drive Systems Using MATLAB GUI," in *MATLAB - A Fundamental Tool for Scientific Computing and Engineering Applications - Volume*, V. Katsikis, Ed., InTech, 2012, pp. 317-342.